Journal of Dental Sciences 20 (2025) 1016–1026

Available online at www.sciencedirect.com

ScienceDirect

journal homepage: www.e-jds.com

Original Article

Optimizing dental implant design: Structure, strength, and bone ingrowth

Jenny Zwei-Chieng Chang [a,b], Jui-Ting Hsu [c,d,e], Ming-Jun Li [f], Hung-Ying Lin [b], Jason Sun [g], Nien-Ti Tsou [f*], Jui-Sheng Sun [h,i**]

[a] School of Dentistry, College of Medicine, National Taiwan University, Taipei, Taiwan
[b] Department of Dentistry, National Taiwan University Hospital, Taipei, Taiwan
[c] School of Dentistry, China Medical University, Taichung, Taiwan
[d] Department of Bioinformatics and Medical Engineering, Asia University, Taichung, Taiwan
[e] School of Dentistry, China Medical University and Hospital, Taichung, Taiwan
[f] Department of Materials Science and Engineering, National Yang Ming Chiao Tung University, Hsinchu, Taiwan
[g] Carmel Catholic High School, One Carmel Parkway, Mundelein, IL, USA
[h] Department of Orthopedic Surgery, Landseed International Hospital, Taoyuan, Taiwan
[i] Department of Orthopedic Surgery, National Taiwan University Hospital, Taipei, Taiwan

Received 17 November 2024; Final revision received 24 November 2024
Available online 6 December 2024

KEYWORDS
Porous;
Finite element analysis;
Biological and mechanical study;
Dental implant design

Abstract *Background/purpose:* Replacing missing teeth with implant-supported prostheses is a common practice; however, function-induced early bone loss may exacerbate peri-implantitis. Identifying factors that influence marginal bone loss is crucial. This study used finite element (FE) simulation and in-vitro analysis to evaluate design concepts and their effects on stresses and strains in dental implants and surrounding bone.
Materials and methods: Five implant designs were analyzed: (1) full solid, (2) upper porous, (3) lower porous, (4) lower porous: upper half, and (5) lower porous: lower half. The study included stability measurements, three-dimensional FE modeling, in-vitro mechanical testing, and simulations of long-term bone remodeling.
Results: The full-solid design showed the highest stress tolerance, followed by the lower porous and upper porous designs. Stress concentration was higher with oblique forces. The upper porous design favored bone strain distribution but exhibited permanent deformation beyond 350 N. Lower porous implants demonstrated similar strength to the full solid but superior marginal bone growth.
Conclusion: Within the scope of this study, the following conclusions were drawn: (1) A well-designed porous structure enhances post-implantation bone growth; (2) An upper porous

* Corresponding author. Department of Materials Science and Engineering, National Yang Ming Chiao Tung University, No. 1001, Daxue Rd. East Dist., Hsinchu City 300093, Taiwan.
** Corresponding author. Department of Orthopedic Surgery, Landseed International Hospital, No. 77, Guangtai Road, Pingzhen District, Taoyuan City 324609, Taiwan.
E-mail addresses: tsounienti@nycu.edu.tw (N.-T. Tsou), drjssun@gmail.com (J.-S. Sun).

https://doi.org/10.1016/j.jds.2024.11.024

design facilitates bone ingrowth but exhibits reduced strength under stress; (3) Lowering porosity adversely affects bone regeneration.

Introduction

Replacing missing teeth with implant-supported prosthesis has become a prevalent choice over the last few decades.[1] Function/stress-induced early bone loss is likely to deepen gingival sulcus/crevice, providing a conducive environment for anaerobic bacteria, further exacerbating bone loss in peri-implantitis.[2] It becomes imperative to identify factors influencing marginal bone loss (MBL). Lessons from the long history of metallic stem prostheses in hip replacements reveal that, in certain cases, bone loss around the implant occurred due to the elasticity mismatch between the bone and the implant, ultimately leading to aseptic loosening.[3,4] To mitigate stress shielding, the Robert Mathys (RM) isoelastic hip prosthesis, featuring a plastic (polyacetyl resin) stem, was introduced in 1970s. Comparison of mechanical consequences of different materials revealed that uncemented femoral stem with modulus similar to that of bone resulted in minimal bone resorption.[4] Long term clinical follow-up of the RM isoelastic design demonstrated better of periprosthetic bone preservation compared to metallic implants.[5] However, discontinued use of the RM isoelastic design was attributed to a high incidence of loosening due to poor bone growth onto the plastic material, large micromotion, absence of osseointegration, poor initial fixation, and increased formation of wear product.[5—8] If the stress shielding effect theory holds true, the manufacture of isoelastic endosseous dental implants should be considered to provide similar elastic properties to the bone, ensuring a secure anchorage for bone ongrowth/ingrowth. Animal studies have shown that using isoelastic material with surface loops or pores results in physiologic stress distribution, better bone regeneration, and avoidance of adverse effects associated with stiff materials on bone remodeling.[9,10]

Previous studies suggest that 3D printed porous dental implants made from titanium-aluminum-vanadium (Ti_6Al_4V; grade V titanium) may be customized to meet patient's need, potentially encouraging bone ingrowth and improving osseointegration by mitigating the mechanical shielding effect.[11,12] However, the increase in porosity may compromise the mechanical properties of the implant. In cases where insufficient bone is available for standard-diameter implant placement, narrow-diameter dental implants offer an alternative option. However, narrow-diameter implants pose potential limitations, structurally weaker and carrying a high risk of fatigue failure.[13] Moreover, the reduced surface area for bone-implant contact may affect the transfer of bone stress and strain, resulting in elevated stress and strains in the surrounding bone.[14] Previous studies have identified implant locations at the maxillary canine and mandibular incisors as risk factors for progressive MBL,[15] areas where narrow-diameter implants are often chosen for implantation. While several studies have examined the biomechanical factors of small-diameter implants,[16,17] none have explored the biomechanical performance of implants with both small diameter and porous design.

Considering that porous design may be a solution to reduce the shielding effect and preserve peri-implant bone, this study aimed to design and fabricate 3D printed Ti6Al4V porous dental implants with small diameters capable of meeting mechanical demands in a worst-case scenario (per ISO 14801:2016). The primary focus was to compare stress and strain distributions under loading on five types of two-piece 3.5 mm-diameter implant with different porous designs and their surrounding bone using finite element (FE) simulation, with the results validated through mechanical tests.

Materials and methods

Implant design

The fundamental configuration of the two-piece 3.5 mm-diameter and 13 mm-length dental implants closely resembled the commercially available Nobel Biocare (Balsberg, Kloten, Switzerland) Implants. The study encompassed five variations with distinct surface porosity: (1) full solid, (2) upper porous, (3) lower porous, and two subtypes, (4) lower porous: upper half, (5) lower porous: lower half implants (Fig. 1A).

Three-dimensional finite element (FE) modeling

The implants geometries were meticulously crafted using computer-aided design software (SolidWorks 2009, SolidWorks Corporation, Concord, MA, USA) and imported into ANSYS Workbench 19.3 (ANSYS, Inc., Canonsburg, PA, USA). The three-dimensional FE model comprised the imported implant, a titanium alloy abutment, a cap, and mandibular bone (19.0 cm × 29.7 cm x 33.5 cm) with a 2-mm thick cortical bone layer constructed from micro-CT images, as shown in Fig. 1B (a). The model underwent meshing using three-dimensional ten-node tetrahedral elements, with s defined region of interest (ROI) around the implant and a specific area around the first three threads (representing the marginal bone area) of the implant for the further analysis [Fig. 1B (b)]. The mesh size was set to be less than or equal to 0.4 mm based on the results of convergence tests.

Material properties, as outlined in Table 1, assumed the entire model to be homogeneous and isotropic elastic.[18,19] The implants and abutment were assigned the material properties of titanium alloy.[18] Frictional contact interfaces

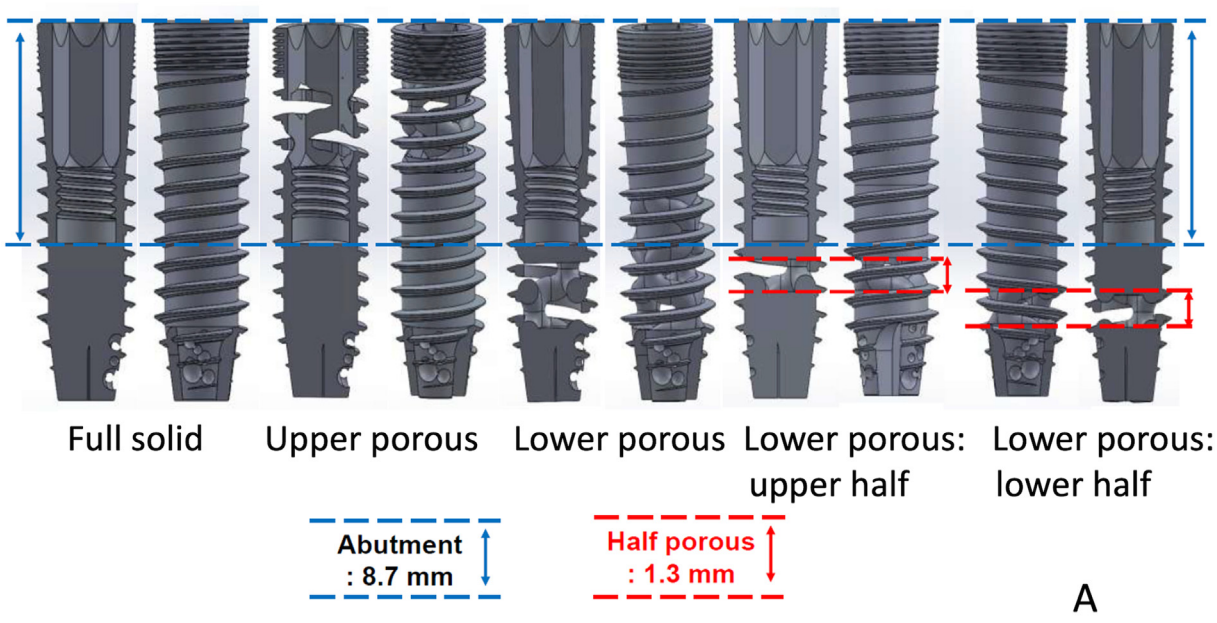

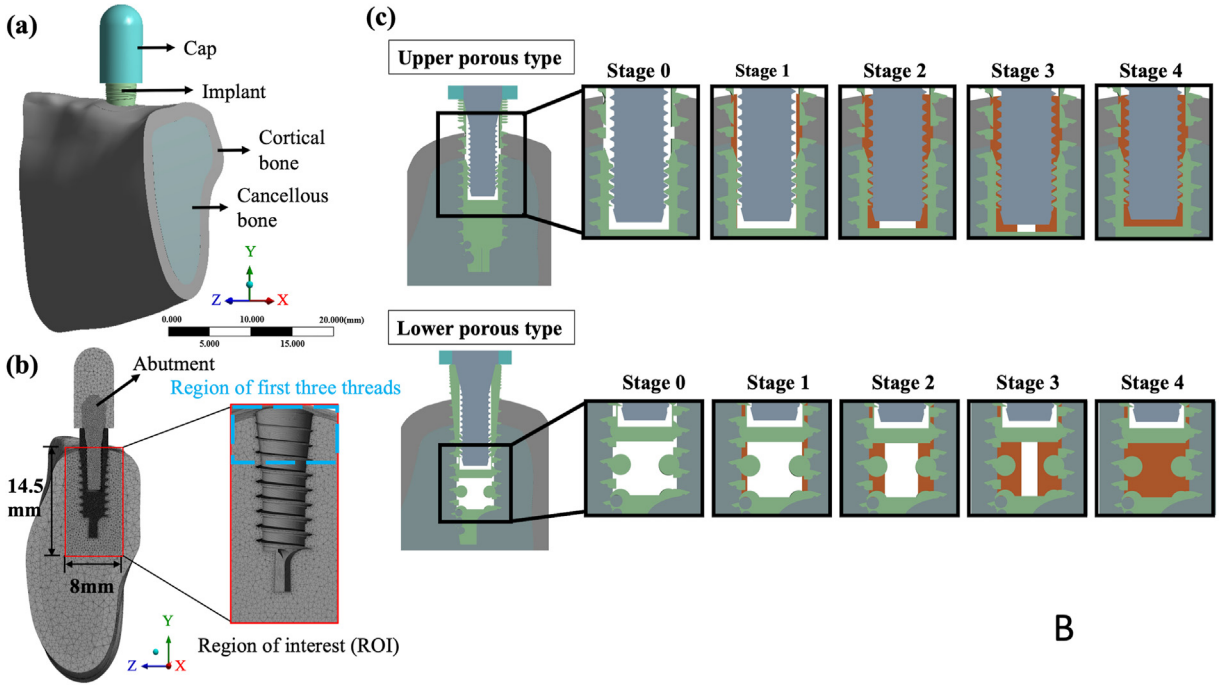

Figure 1 Five implant designs and three-dimensional finite element (FE) analysis models of the implant body and its surrounding bone.

A: Five implant designs. Three major types: (1) full solid, (2) upper porous, (3) lower porous, and two subtypes: (4) lower porous: upper half, and (5) lower porous: lower half implants.

B: Three-dimensional finite element (FE) analysis models of the implant body and its surrounding bone. (a) The entire three-dimensional FE model, including a sectional view; (b) A cross-sectional diagram of the three-dimensional mesh model. The area delineated by the red line corresponds to the region of interest (ROI). The blue-dotted line outlines the extent of the first three threads (representing the marginal bone area). (c) Simulation of the early bone growth process, encompassing Stages 0—4. The orange region indicates the filled bone during each stage.

Table 1 Material properties used in the finite element model.

Materials	Young's modulus (MPa)	Poisson's ratio: ν
Structural steel	200,000	0.3
Titanium alloy (Ti_6Al_4V)	96,000	0.36
Cortical bone	10,700	0.3
Cancellous bone	910	0.3
Fibrous tissue	2	0.17

Abbreviations: MPa, megapascals; Ti_6Al_4V, titanium alloy with 6 % aluminum and 4 % vanadium.

were established between the bone and other components with a frictional coefficient of 0.1. The mesial and distal surfaces of the bone were constrained. Two loading scenarios were considered: (1) Vertical loading with a force of 150 N applied onto the top of the cap along the -y direction, and (2) Oblique loading, incorporating a lateral buccal to lingual side force of 20 N in addition to the vertical force.[20]

Simulation of bone growth and remodeling spanned six stages, starting from Stage 0 (immediately post-implantation with no bone growth) to Stage 4 (complete filling with bone). Fig. 1B (c) illustrated the simulation of the early bone growth for the upper and lower porous implants. The 's/p bone remodeling' stage represented the long-term status of post-surgery (s/p) bone remodeling after implantation. Based on the theories of Minimum Effective Strain (MES) and the mechanostat theories proposed by Harold Frost,[21–25] strain responses categorized bone reactions into "over yield point," "bone gain," "adapted," and "bone loss." By adjusting Young's modulus according to these categories, the strain and stress distributions of the modified model were calculated to simulate s/p bone remodeling under the same conditions as Stage 4.

For the outcomes derived from the Stage 0–4 models and s/p bone remodeling, an assessment was conducted on the volume fractions of healthy and diseased bone around the implant in the ROI. In this context, healthy bone encompassed elements with strain falling within the "bone gain" and "adapted" ranges, while diseased bone was defined as those with strain in the "over yield point" and "bone loss" ranges. It was assumed that a higher volume fraction of healthy bone and a lower volume fraction of diseased bone would indicate superior implant performance.

Dynamic loading test for laser-sintered Ti_6Al_4V dental implants

The three primary implant types (full solid, upper porous, lower porous) were fabricated using the laser-sintered additive technique as previously described.[11,12] Failure evaluation of the implants was conducted using a material testing machine (JSV-H1000, Japan Instrumentation System, Nara, Japan). Fatigue testing followed the procedures outlined in the dynamic loading test for dental implants as per ISO 14801 requirements. A custom-made jig constrained the sample on the testing platform of the loading machine. At least three specimens for each design met the ISO 14801 standards without failures, after which subsequent experiments were conducted. Detailed records of the failure mode and photographs of the failed implants were documented.

Bone specimen preparation

For this study, the density of trabecular bone chosen simulated Type 2 bone, following Misch's bone-density classification.[26] A Sawbone model of trabecular bone (density: 0.4 g/cm^3, elastic modulus: 759 MPa; model 1522-05) (Pacific Research Laboratories, Vashon Island, WA, USA) was used, featuring a 2-mm thick synthetic cortical layer (elastic modulus: 16.7 GPa; model 3401-02) (Pacific Research Laboratories). The synthetic bone block, rectangular in shape, measured 41 mm × 30 mm x 43.5 mm in dimension.

Implant stability measurement

The Periotest device (Periotest Classic, Medizintechnik Gulden, Modautal, Germany) gauged the mobility of the three major types of laser-sintered Ti_6Al_4V dental implants after the implants post-insertion into the bone blocks. Positioned perpendicularly 2 mm from the abutment, the measurement device's tip delivered impacts to the implant at a rate of four times per second for a duration of 4 s, after which Periotest values (PTVs) were measured.[27]

Statistical analysis

Both implant stability and peak minimum principal strains under loading were measured, and the results were summarized as median and interquartile range values. Comparisons between these implant systems were analyzed with Wilcoxon's rank-sum test with commercial statistical software (SAS version 9.1, SAS Institute, Cary, NC, USA) with a significant value of 0.05.

Results

Mechanical experiments

Examining the load–deformation curve, the full-solid design exhibited the highest tolerance, followed by lower porous design, while the upper porous design possessed the lowest stress tolerance (Fig. 2A). In the measurement of implant stability, the smaller the periotest values (PTV), the higher the stability.[28] Across all three different designs, the PTV consistently demonstrated excellent stability. However, discernible differences were noted among the groups, with the stability of full solid and upper porous designs surpassing that of lower porous design (Fig. 2A).

Failure characteristics of implant assemblies

For the upper porous design, permanent deformation occurred when the applied force exceeded 350 N. Removal of the cap revealed a crooked internal screw beneath the abutment (Fig. 2B). This area displayed a distinct

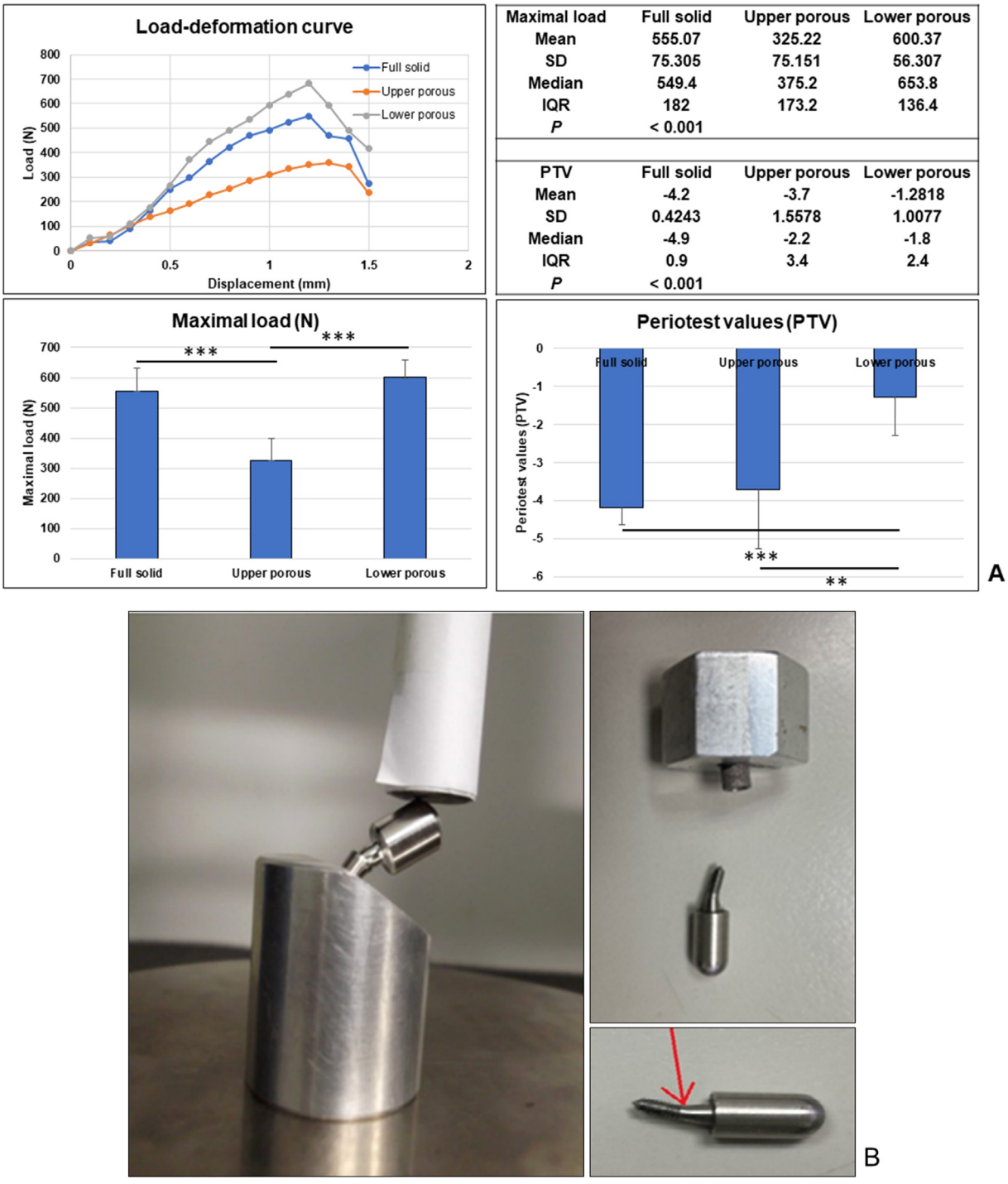

Maximal load	Full solid	Upper porous	Lower porous
Mean	555.07	325.22	600.37
SD	75.305	75.151	56.307
Median	549.4	375.2	653.8
IQR	182	173.2	136.4
P	< 0.001		

PTV	Full solid	Upper porous	Lower porous
Mean	-4.2	-3.7	-1.2818
SD	0.4243	1.5578	1.0077
Median	-4.9	-2.2	-1.8
IQR	0.9	3.4	2.4
P	< 0.001		

Figure 2 The load—deformation curves, periotest values (PTV) of the various implant designs and Failure characteristics of implant assemblies.

A: The load—deformation curves and periotest values (PTV) of the various implant designs. The load—deformation curve revealed that the full-solid design exhibited the highest tolerance to stress, followed by lower porous design, with the upper porous design showing the lowest stress tolerance. Regarding periotest values (PTV), all three designs demonstrated excellent stability, with the lower porous design exhibiting the least stability. (N = 11; **: $P < 0.01$, ***: $P < 0.001$)

B: Failure characteristics of implant assemblies.

In the upper porous design, visible permanent deformation became apparent when the applied force exceeded 350 N. Upon disassembly, it was observed that the internal screw under the abutment was crooked.

Abbreviations: IQR, interquartile range; *P*, probability value; SD, standard deviation.

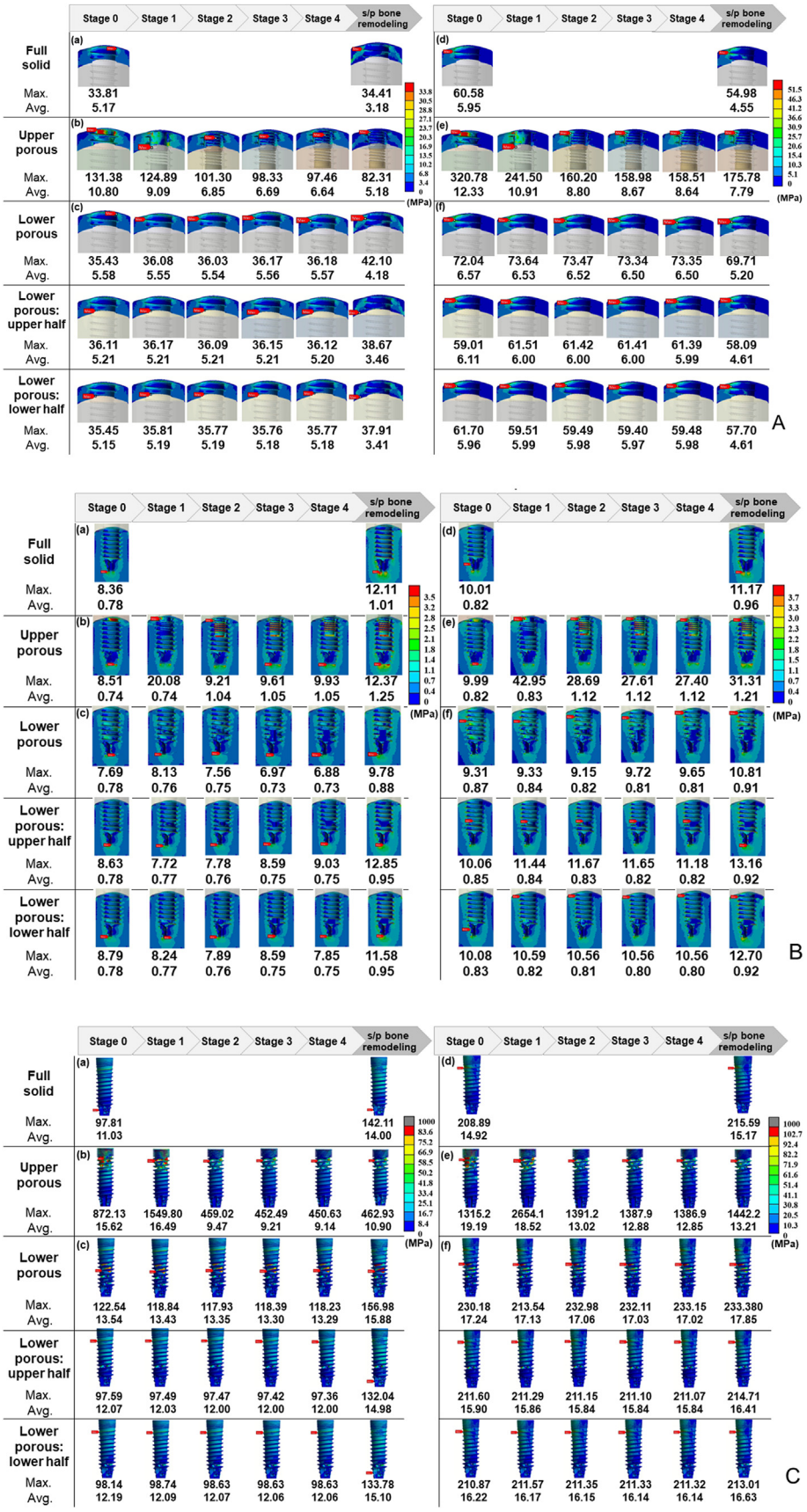

Figure 3 Maximum and average stress distribution in cortical bone **(A)**, cancellous bone **(B)** and implant body **(C)**.
A: Maximum and average stress distribution in cortical bone, encompassing Stages 0—4 and post-surgery (s/p) bone remodeling.

discontinuity in geometric shape, leading to stress concentration and, consequently, the initial deformation at this site.

Three-dimensional FE analysis: simulations of immediate post-implantation conditions

When a vertical force of 150 N was applied, the cortical bone's highest stress occurred around the necks of all three designs [Fig. 3A (a—c)]. The upper porous implant exhibited the highest stress in the cortical bone [131.38 MPa in Fig. 3A (b)]. Stress in the cancellous bone peaked around the apical tip of the implants, showing comparable maximum and average values for all three designs [Fig. 3B (a—c)]. Notably, the lower porous implant demonstrated a more uniform stress distribution in contrast to the full-solid and upper porous implants [Fig. 3B (c)].

For the implant body, the maximum stress occurred at the apical tip of the full solid implant [Fig. 3C (a)], whereas it took place at the top interface between the solid and porous portions in the upper porous and lower porous implants [Fig. 3C (b) and (c), respectively]. The upper porous design introduced higher stress in the cortical bone layer, with the maximum stress on the upper porous implant body (872.13 MPa) significantly exceeding that on the full-solid (97.81 MPa) and lower porous (122.54 MPa) implants. This elevated stress was attributed to the sharp corners of the helical structure [Fig. 3C (b)].

Under oblique loads, the stress distribution shifted towards the side opposite to the direction of force application [Fig. 3A—C (d—f)], with an overall increase stress magnitude, particularly within the implant body. The upper porous implant experienced the highest stress value [1315.2 MPa, Fig. 3C (e)] among the three designs, attributed to significant bending at the interface between the solid and porous portions, possibly leading to mechanical failures. The stress distribution trends under the oblique loads mirrored those under vertical loads.

Three-dimensional FE analysis: simulations for bone growth and remodeling

Fig. 4(a—c) illustrated the distribution of healthy and diseased bone for the three implants under vertical loads. Bone loss typically occurred around the threads and bone gain occurred at the tip. Table 1 presented volume fractions of healthy and disease bone around the first three threads (the marginal bone area). The upper (78.2 %) and lower porous (74.3 %) implants outperformed the full solid implant (69.5 %) in terms of volume fraction of healthy bone. Additionally, the volume fractions of diseased bone around the first three threads of the upper (21.8 %) and lower porous (25.7 %) implant were lower than that in full solid implant (30.5 %). These findings indicated superior performance of both the upper and lower porous implants under vertical loads.

Fig. 4(d—f) demonstrated that bone loss typically occurred in the cortical bone layer near the site of oblique force application. Table 2 highlighted that the volume fractions of healthy bone around the first three threads of the upper, lower porous, and full solid implants were 65.7 %, 59.0 %, and 57.3 %, respectively, while those of diseased bone were 34.3 %, 41.0 %, and 42.7 %, respectively. These results indicated that the superior performance of both the upper and lower porous implants compared to the full solid implant under oblique loads.

Discussion

The onset and progression of peri-implant bone loss has been extensively documented in the literature, with various measurements and disease thresholds used to diagnose peri-implant disease. Numerous studies have focused on MBL within the first year of dental implant in function,[29,30] and consensus statements often consider radiographic crestal bone loss of less than 2 mm from initial implant insertion surgery as successful outcome.[2] We speculate that the mismatch of elasticity between bone and implant is suspected to contribute to early MBL, akin to observations in orthopedics. The FE analysis supports this concept, showing that the maximum stress in the cortical bone concentrates around the neck under vertical loading, while bone loss occurs in the cortical layer near the site of oblique force application. Notably, the solid implant exhibited the lowest volume fractions of healthy bone and higher volume fractions of diseased bone around the initial three threads when subjected to both vertical and oblique loads. A 10-year prospective cohort study demonstrated the importance of addressing early bone loss, as implants with early bone loss $\geq$0.5 mm during the first year of function have a significantly higher likelihood of developing future peri-implantitis.[31] To mitigate potential complications associated with conventional implants, the development of isoelastic dental implants with enhanced osseointegration capabilities becomes imperative.

The fatigue strength of the small-diameter implants, particularly those below 3 mm, is markedly lower,[13] posing a fracture risk in clinical practice. Implant diameter plays a crucial role in determining its ability to withstand repeated stress over time. Our study aims to enhance the biomechanical performance of two-piece 3.5 mm-diameter

(a)—(c) Stress results under vertical loads;
(d)—(f) stress results under oblique loads.
B: Maximum and average stress distribution in cancellous bone, encompassing Stages 0—4 and post-surgery (s/p) bone remodeling.
(a)—(c) Stress results under vertical loads;
(d)—(f) stress results under oblique loads.
C: Maximum and average stress distribution in implant body, encompassing Stages 0—4 and post-surgery (s/p) bone remodeling.
(a)—(c) Stress results under vertical loads;
(d)—(f) stress results under oblique loads.
Abbreviations: Avg, average; Max, maximum; s/p, post-surgery.

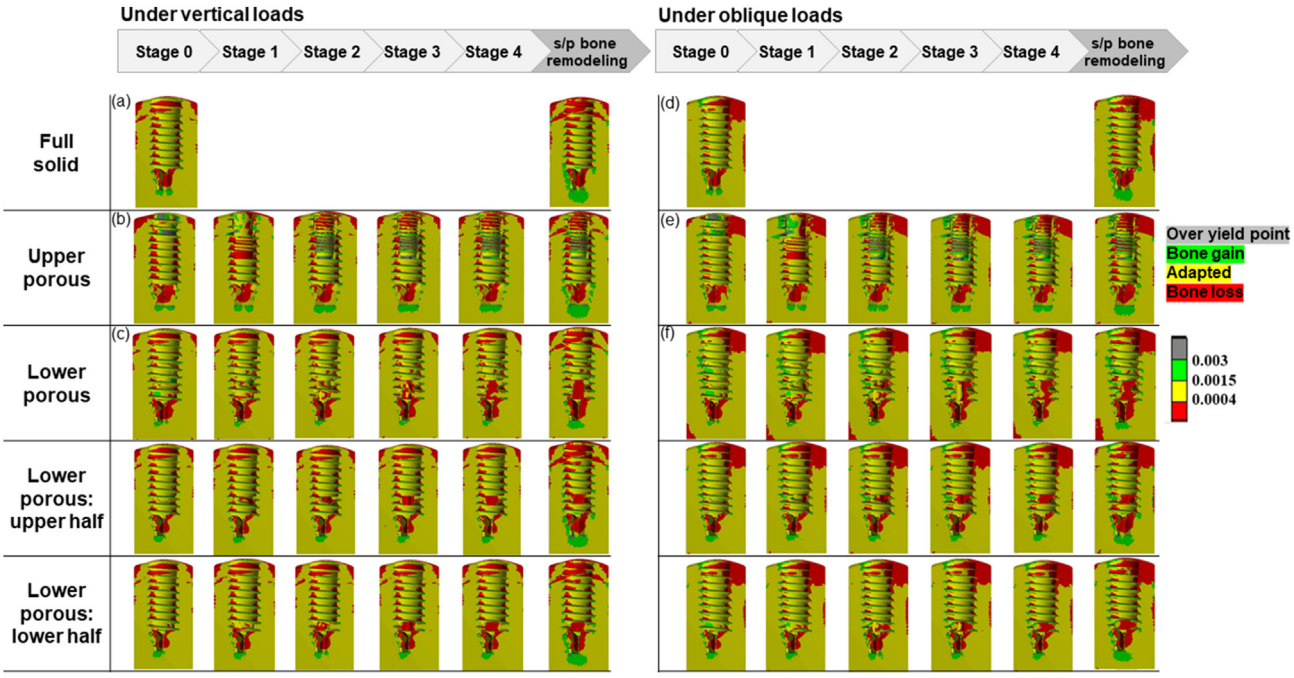

Figure 4 The distribution of healthy and diseased bone for the five implant designs, encompassing Stages 0–4 and post-surgery (s/p) bone remodeling. (a–c) results under vertical loads; (d–f) results under oblique loads.

implants by comparing various porous designs through FE analyses. Our findings highlight that, despite the upper porous design exhibiting the highest volume fractions of healthy bone and the lowest volume fractions of diseased bone around the first three threads (the marginal bone area) under loading, it experienced maximum stress at the top interface between the solid and porous portions of the implant body. This maximum stress was significantly exceeded that of other designs, reaching over 1300 MPa under oblique loads, potentially leading to mechanical failures. This stress concentration issue was confirmed by mechanical tests, where upper porous implants displayed permanent deformation when the applied force exceeded 350 N. Consequently, although the upper porous design encourages better bone ingrowth, its inability to withstand mechanical tests due to stress concentration at the solid-porous junction makes it unsuitable for clinical practice. This limitation may persist even after full regeneration of bone ingrowth and during subsequent bone remodeling. Consequently, the upper porous implant may not be suitable for clinical practice. To address this, improvements in the upper porous design's connection, influencing both stability and the strength of the titanium grade material,[32] are necessary to enhance resistance to deformation under static overloading.

Various mechanical and biological factors, including principal tensile strain, hydrostatic stress, hydro-static pore pressure, deviatoric strain, and fluid flow, have been considered pivotal for achieving an accurate and more realistic tissue differentiation process. Mechano-regulation theories, assessing bone remodeling in response to diverse mechanical stimuli, have been proposed by scientists.[33] Research indicates that a single parameter, deviatoric strain, can effectively simulate the tissue (callus) differentiation process.[34] Building upon our previous study, where a mechano-regulation algorithm implemented by finite element models to accurately predict tissue differentiation around or within the porous implants,[18] we applied a similar algorithm in this study to enhance the design efficiency and minimize the need for animal sacrifices. In contrast to the upper porous design, our results revealed that the lower porous did not lead to stress concentration within the implant body, making it more clinically desirable due to specific geometric shapes. While stress values in the cortical layer and cancellous bone surrounding the lower porous design were comparable to those of full solid implant under loading, the stress distribution in the lower porous implant was more uniform, displaying a blend of light and dark blue regions. Although the volume fractions of healthy and diseased bone around the entire implant body in the ROI between solid and lower porous implants under loading were very similar, the volume fraction of healthy bone for the first three threads was higher for the lower porous implant compared to the full solid implant. This difference became more pronounced in the s/p bone remodeling stage. However, regardless of the implant design, in the post-surgery (s/p) bone remodeling stage, the proportion of healthy bone decreased, while the proportion of diseased bone increased compared to the early bone growth stage (Stages 0–4). Most of the adapted bone turned into bone loss, particularly evident in the lower porous: upper and lower half variants. Diseased bone increased by more than 20 %, especially at the first three threads of the lower porous: lower half design when under the vertical load. Consequently, bone ongrowth/ingrowth is more favorable in the lower porous design compared to the full solid type and it demonstrates similar mechanical strength to the full solid type. However, this effect diminishes if we reduce the volume of the porous portion.

Table 2 The volume fractions of healthy and diseased bone at each stage. The total bone within the region of interest showed similar volume fractions of healthy bone, with differences of approximately 2∼3 %, across all implant designs. During post-surgery (s/p) bone remodeling stage, the volume fractions of healthy bone surpassed 50 % in both the upper porous and lower porous designs at the first three threads (representing the marginal bone area).

Implant type	Simulation stage	Under vertical loads				Under oblique loads			
		Healthy		Diseased		Healthy		Diseased	
		(Bone gain + adapted)		(Over yield point + bone loss)		(Bone gain + adapted)		(Over yield point + bone loss)	
		Total	First 3 threads	Total	First 3 threads	Total	First 3 threads	Total	First 3 threads
Full solid	Stage 0	80.6	69.5	19.4	30.5	78.3	57.3	21.7	42.7
	After bone remodeling	73.4	45.5	26.6	54.5	74.4	48.6	25.6	51.4
Upper porous	Stage 0	79.8	78.2	20.2	21.8	80.3	65.7	19.7	34.3
	Stage 1	77.3	79.1	22.7	20.9	76.1	67.4	23.9	32.6
	Stage 2	77.8	76.9	22.2	23.1	77.0	68.8	23.0	31.2
	Stage 3	76.5	75.8	23.5	24.2	76.4	68.4	23.6	31.6
	Stage 4	77.1	75.4	22.9	24.6	76.6	68.2	23.4	31.8
	After bone remodeling	70.9	64.0	29.1	36.0	72.8	61.2	27.2	38.8
Lower porous	Stage 0	81.4	74.3	18.6	25.7	79.2	59.0	20.8	41.0
	Stage 1	80.4	74.1	19.6	25.9	78.8	58.9	21.2	41.1
	Stage 2	80.4	74.0	19.6	26.0	78.1	58.8	21.9	41.2
	Stage 3	79.0	74.2	21.0	25.8	76.7	58.7	23.3	41.3
	Stage 4	79.4	74.2	20.6	25.8	76.8	58.7	23.2	41.3
	After bone remodeling	73.5	56.9	26.5	43.1	72.4	51.3	27.6	48.7
Lower porous: Upper half	Stage 0	81.3	71.1	18.7	28.9	77.2	55.8	22.8	44.2
	Stage 1	80.9	71.0	19.1	29.0	76.9	55.6	23.1	44.4
	Stage 2	80.3	71.1	19.7	28.9	76.2	55.9	23.8	44.1
	Stage 3	78.5	71.0	21.5	29.0	75.1	55.7	24.9	44.3
	Stage 4	78.9	70.9	21.1	29.1	75.3	55.6	24.7	44.4
	After bone remodeling	70.9	47.3	29.1	52.7	70.8	47.2	29.2	52.8
Lower porous: Lower half	Stage 0	80.2	70.2	19.8	29.8	77.8	56.1	22.2	43.9
	Stage 1	80.7	70.7	19.3	29.3	78.2	56.5	21.8	43.5
	Stage 2	80.2	70.7	19.8	29.3	77.2	56.4	22.8	43.6
	Stage 3	78.9	70.6	21.1	29.4	76.4	56.4	23.6	43.6
	Stage 4	79.2	70.6	20.8	29.4	76.5	56.4	23.5	43.6
	After bone remodeling	71.1	46.7	28.9	53.3	71.9	47.9	28.1	52.1

Limitation of this study include the use of a simplified bone shape, as strain patterns can vary with bone geometry, such as the complex nature of bone remodeling and the variability of loading conditions in vivo. The overly simplified model may not fully capture the porous nature and complex material properties of bone, such as inhomogeneity, anisotropy, and viscoelasticity. Future finite element studies should aim for more sophisticated simulations that accurately represent the shape and material properties of bone to reduce inconsistencies between simulated and experimentally measured surface strains. Additional limitation is that, the study applied only static occlusal forces (vertical and oblique) in both mechanical experiments and finite element simulations, assuming lateral force represents a realistic occlusal direction.[35] Future investigations incorporating chewing simulations should consider the presence of sliding and friction phenomena during mastication.[36]

In summary, meticulous consideration of the implant's structural characteristics is crucial for optimal performance in both biological and mechanical aspects. Within the scope of this study, the conclusions are outlined: (1) A well-designed porous structure significantly enhances post-implantation bone ongrowth and ingrowth; (2) An upper porous design demonstrates superior bone integration but shows reduced stress resistance during mechanical testing in a 3.5 mm-diameter two-piece implant; and (3) Reducing porous proportion negatively impacts bone regeneration. Achieving an optimized design is crucial to balance mechanical strength and bone integration effectively. Here, we have demonstrated areas for future research that could help elucidate the mechanisms driving bone resorption, such as incorporating biological models or dynamic loading conditions in future simulations. In the future, the use of advanced materials (e.g., titanium alloys, bioactive coatings, or polymer-composite hybrids) and hybrid structures (e.g., combining porous and solid sections) may have the potential to improve the balance between mechanical strength and biological performance.

Declaration of competing interest

The authors have no conflicts of interest relevant to this article.

Acknowledgement

All works were performed at National Taiwan University, National Taiwan University Hospital (Taipei, Taiwan) and National Yang Ming Chiao Tung University (Hsinchu, Taiwan).

References

1. Elani HW, Starr JR, Da Silva JD, Gallucci GO. Trends in dental implant use in the U.S., 1999-2016, and projections to 2026. *J Dent Res* 2018;97:1424—30.
2. Misch CE, Perel ML, Wang HL, et al. Implant success, survival, and failure: the International Congress of Oral Implantologists (ICOI) Pisa Consensus Conference. *Implant Dent* 2008;17:5—15.
3. Rotem A. Effect of implant material properties on the performance of a hip joint replacement. *J Med Eng Technol* 1994;18:208—17.
4. Weinans H, Huiskes R, Grootenboer HJ. Effects of material properties of femoral hip components on bone remodeling. *J Orthop Res* 1992;10:845—53.
5. Nagi ON, Kumar S, Aggarwal S. The uncemented isoelastic/isotitan total hip arthroplasty. A 10-15 years follow-up with bone mineral density evaluation. *Acta Orthop Belg* 2006;72:55—64.
6. Trebse R, Milosev I, Kovac S, Mikek M, Pisot V. Poor results from the isoelastic total hip replacement: 14-17-year follow-up of 149 cementless prostheses. *Acta Orthop* 2005;76:169—76.
7. Thiagarajan P, Das De S. Severe metallosis in an isoelastic hip prosthesis. *Singap Med J* 1998;39:324—5.
8. Izquierdo RJ, Northmore-Ball MD. Long-term results of revision hip arthroplasty. Survival analysis with special reference to the femoral component. *J Bone Joint Surg Br* 1994;76:34—9.
9. Breme J, Biehl V, Schulte W, d'Hoedt B, Donath K. Development and functionality of isoelastic dental implants of titanium alloys. *Biomaterials* 1993;14:887—92.
10. Tarvainen T, Paronen I, Tunturi T, et al. Bone remodelling in the pores and around load bearing transchondral isoelastic porous-coated glassy carbon implants: experimental study in rabbits. *J Mater Sci Mater Med* 1998;9:509—15.
11. Chang JZ, Tsai PI, Kuo MY, Sun JS, Chen SY, Shen HH. Augmentation of DMLS biomimetic dental implants with weight-bearing strut to balance of biologic and mechanical demands: from bench to animal. *Materials* 2019;12:164.
12. Tu CC, Tsai PI, Chen SY, Kuo MY, Sun JS, Chang JZ. 3D laser-printed porous Ti(6)Al(4)V dental implants for compromised bone support. *J Formos Med Assoc* 2020;119:420—9.
13. Allum SR, Tomlinson RA, Joshi R. The impact of loads on standard diameter, small diameter and mini implants: a comparative laboratory study. *Clin Oral Implants Res* 2008;19:553—9.
14. Qian J, Wennerberg A, Albrektsson T. Reasons for marginal bone loss around oral implants. *Clin Implant Dent Relat Res* 2012;14:792—807.
15. Sun JS, Liu KC, Hung MC, et al. A cross-sectional study for prevalence and risk factors of peri-implant marginal bone loss. *J Prosthet Dent* 2023 Nov 29. https://doi.org/10.1016/j.prosdent.2023.11.002. S0022-3913(23)00722-9. Online ahead of print. PMID: 38036320.
16. Wu AY, Huang HL, Hsu JT, Chee W. Biomechanical effects of the implant material and implant-abutment interface in immediately loaded small-diameter implants. *Clin Oral Invest* 2014;18:1335—41.
17. Wu AY, Hsu JT, Chee W, Lin YT, Fuh LJ, Huang HL. Biomechanical evaluation of one-piece and two-piece small-diameter dental implants: in-vitro experimental and three-dimensional finite element analyses. *J Formos Med Assoc* 2016;115:794—800.
18. Huang CC, Li MJ, Tsai PI, et al. Novel design of additive manufactured hollow porous implants. *Dent Mater* 2020;36:1437—51.
19. Aversa R, Apicella D, Perillo L, et al. Non-linear elastic three-dimensional finite element analysis on the effect of endo-crown material rigidity on alveolar bone remodeling process. *Dent Mater* 2009;25:678—90.
20. Steiner M, Mitsias ME, Ludwig K, Kern M. In vitro evaluation of a mechanical testing chewing simulator. *Dent Mater* 2009;25:494—9.
21. Feng X, McDonald JM. Disorders of bone remodeling. *Annu Rev Pathol* 2011;6:121—45.
22. Frost HM. A determinant of bone architecture. The minimum effective strain. *Clin Orthop Relat Res* 1983:286—92.
23. Frost HM. Bone "mass" and the "mechanostat": a proposal. *Anat Rec* 1987;219:1—9.
24. Kan JP, Judge RB, Palamara JE. In vitro bone strain analysis of implant following occlusal overload. *Clin Oral Implants Res* 2014;25:e73—82.

25. Frost HM. Bone's mechanostat: a 2003 update. *Anat Rec A Discov Mol Cell Evol Biol* 2003;275:1081—101.
26. Chong L, Khocht A, Suzuki JB, Gaughan J. Effect of implant design on initial stability of tapered implants. *J Oral Implantol* 2009;35:130—5.
27. Alsaadi G, Quirynen M, Michiels K, Jacobs R, van Steenberghe D. A biomechanical assessment of the relation between the oral implant stability at insertion and subjective bone quality assessment. *J Clin Periodontol* 2007;34:359—66.
28. Chakrapani S, Goutham M, Krishnamohan T, Anuparthy S, Tadiboina N, Rambha S. Periotest values: its reproducibility, accuracy, and variability with hormonal influence. *Contemp Clin Dent* 2015;6:12—5.
29. Oh TJ, Yoon J, Misch CE, Wang HL. The causes of early implant bone loss: myth or science? *J Periodontol* 2002;73:322—33.
30. Galindo-Moreno P, Leon-Cano A, Ortega-Oller I, Monje A, F OV, Catena A. Marginal bone loss as success criterion in implant dentistry: beyond 2 mm. *Clin Oral Implants Res* 2015;26:e28—34.
31. Windael S, Collaert B, De Buyser S, De Bruyn H, Vervaeke S. Early peri-implant bone loss as a predictor for peri-implantitis: a 10-year prospective cohort study. *Clin Implant Dent Relat Res* 2021;23:298—308.
32. Park SJ, Lee SW, Leesungbok R, Ahn SJ. Influence of the connection design and titanium grades of the implant complex on resistance under static loading. *J Adv Prosthodont* 2016;8:388—95.
33. Metz C, Duda GN, Checa S. Towards multi-dynamic mechano-biological optimization of 3D-printed scaffolds to foster bone regeneration. *Acta Biomater* 2020;101:117—27.
34. Cheong VS, Fromme P, Mumith A, Coathup MJ, Blunn GW. Novel adaptive finite element algorithms to predict bone ingrowth in additive manufactured porous implants. *J Mech Behav Biomed Mater* 2018;87:230—9.
35. Geng JP, Tan KB, Liu GR. Application of finite element analysis in implant dentistry: a review of the literature. *J Prosthet Dent* 2001;85:585—98.
36. Murakami N, Wakabayashi N. Finite element contact analysis as a critical technique in dental biomechanics: a review. *J Prosthodont Res* 2014;58:92—101.